*J Neurophysiol* 91: 1794–1807, 2004.
First published December 10, 2003; 10.1152/jn.00574.2003.

# Functional Connectivity of Disparity-Tuned Neurons in the Visual Cortex

**Michael D. Menz and Ralph D. Freeman**
*Group in Vision Science, School of Optometry, and Helen Wills Neuroscience Institute, University of California, Berkeley, California 94720-2020*

Submitted 13 June 2003; accepted in final form 28 November 2003

**Menz, Michael D. and Ralph D. Freeman.** Functional connectivity of disparity-tuned neurons in the visual cortex. *J Neurophysiol* 91: 1794–1807, 2004. First published December 10, 2003; 10.1152/jn.00574.2003. Different mechanisms have been proposed concerning how disparity-tuned neurons might be connected to produce the signals for depth perception. Here we present neurophysiological evidence providing insight on this issue. We have recorded simultaneously from pairs of disparity-tuned neurons in the cat's striate cortex. The purpose was to determine the relationships between disparity tuning and functional connectivity revealed through neural cross-correlograms. Monosynaptic connections tend to be stronger between pairs of cells with similar disparity tuning. Pairs of complex cells tend to have either similar tuning or nearly opposite tuning with an absence of quadrature relations. Pairs with at least one simple cell do have some nearly quadrature relationships when they are recorded from the same electrode. Coarse-to-fine connections (i.e., the presynaptic cell has lower disparity frequency and larger disparity range) tend to be stronger but less frequent than those of a fine-to-coarse nature. Our results are consistent with a system that produces weighted averaging across cells that are tuned to similar disparities but different disparity scales to reduce false matches.

## INTRODUCTION

The transmission of information in central visual pathways undergoes two major transformations in the striate cortex. First, receptive fields (RFs) generally lose concentric center-surround organization. Second, signals from left and right eyes are combined to form a neural substrate for binocular vision. The lateral displacement of the eyes creates a horizontal image disparity. When these images are properly fused, the normal binocular system creates a perception of stereoscopic depth. The neural basis of this function has been investigated by theoretical, behavioral, and neurophysiological approaches. The first relevant physiological finding was that cells in V1 (area 17) respond to different depth planes. (Barlow et al. 1967; Nikara et al. 1968). Studies in awake behaving monkeys confirmed and expanded this finding (e.g., Poggio 1990; Poggio and Fischer 1977; Poggio et al. 1985).

None of the early neurophysiological studies was concerned with neural mechanisms. It was tacitly assumed that RFs with lateral displacements were disparity detectors. Furthermore, left and right RFs were thought to be identical (Hubel and Wiesel 1962) so that lateral displacement made sense as an encoding mechanism. More recent work has shown that differences in internal RF structure or phase between left and right eyes constitute an important encoding mechanism. This has been demonstrated in anesthetized paralyzed cats (Anzai et al. 1997; DeAngelis et al. 1992, 1995; Freeman and Ohzawa 1990, 1992; Ohzawa et al. 1996, 1997) and in awake behaving monkeys (Cumming and Parker 1999, 2000). In addition, a disparity-encoding scheme, based on the energy model (Adelson and Bergen 1985; Watson and Ahumada 1985), has been developed under the assumption of serial processing from simple-to-complex cells (Ohzawa et al. 1990, 1997).

Although these studies of mechanisms are illuminating, a number of questions remain. One important area concerns the combination and transmission of stereoscopic information. There are two variables relevant to spatial scale; disparity frequency and disparity range. Disparity frequency is important because visual scenes contain a wide variety of detail, and neurons are selectively responsive to specific spatial bands. Disparity information must therefore be combined across spatial scale. Disparity range is relevant because of a trade-off with frequency. Coarse stereopsis can occur over a wide range of depths. Fine stereopsis provides the required resolution but is limited to a small range. A central question is: how does stereoscopic processing occur so that different spatial scales are combined to provide coarse and fine levels? In the preceding paper, we addressed this question using two types of neurophysiological analysis. First, we found that disparity tuning generally sharpens during the time course of the response. Second, we determined that neurons tuned to large spatial scale have relatively short temporal latencies (Menz and Freeman 2004). Both these findings are consistent with a coarse-to-fine neural processing sequence. In the study reported here, we have examined this topic by carrying out an analysis of simultaneous extracellular recordings from pairs of neurons in striate cortex. Both sparse and dense noise visual stimulation were used to obtain disparity-tuning curves for simple and complex cells. (Anzai et al. 1999a–c; Ohzawa et al. 1996, 1997) Cross-correlations between pairs of neurons were analyzed to determine functional intercellular relationships for disparity-tuned neurons.

We have determined several types of relationships between disparity-tuned cortical cells. The most important concerns the connections between disparity frequency and range. The most common connection is one in which the presynaptic cell of the pair has a relatively high disparity frequency. However, cross-correlograms are generally stronger for pairs in which the presynaptic cell is lower in disparity frequency. Considered together, this combination of findings and the results reported in the preceding paper (Menz and Freeman 2004) are expected for a system in which there is a weighted averaging across spatial scale, and coarse processing occurs prior to fine. This type of coarse-to-fine process has been proposed in theoretical

Address for reprint requests and other requests: R. D. Freeman, 360 Minor Hall, University of California, Berkeley, CA 94720-2020 (E-mail: freeman@neurovision.berkeley.edu).

The costs of publication of this article were defrayed in part by the payment of page charges. The article must therefore be hereby marked "*advertisement*" in accordance with 18 U.S.C. Section 1734 solely to indicate this fact.

  

work as a solution to the correspondence problem (Marr and Poggio 1979). A similar mechanism may apply to overall stereoscopic processing and to other perceptual events.

## METHODS

Experiments are conducted with anesthetized, paralyzed cats. The equipment and procedures for surgery, animal maintenance, single-unit recording, RF mapping, and some data analysis techniques have been described in previous papers from our laboratory (Anzai et al. 1999a,b; DeAngelis et al. 1993a,b, 1999; Ohzawa et al. 1997). The following narrative emphasizes procedures that are most relevant to the current study.

### *Surgical procedures and animal maintenance*

The surgical and animal maintenance procedures are described in detail in the preceding companion paper (Menz and Freeman 2004). Experiments lasted for 3–4 days. At the end of the experiment, animals are killed with pentobarbital sodium (Nembutal, ~50 mg/kg). The animal is immediately perfused with a formaldehyde solution. Electrode tracks are reconstructed and cortical lamina identified. Recordings were made at all depths and all cells were recorded from area 17.

### *Experimental apparatus*

Visual stimuli are generated by a computer with two high-resolution graphics boards. Images are displayed on a pair of video monitors, one for each eye, that the cat views by means of beam splitters. The mean luminance of the displays viewed through the beam splitters is 23 cd/m$^2$. In one recording configuration, two tungsten-in-glass or varnished tungsten microelectrodes are advanced together into visual cortex via a piezoelectric micropositioner. The lateral tip spacing is ~250 $\mu$m for the varnished tungsten and ~350 $\mu$m for the tungsten-in-glass electrodes. Vertical position tip differences are ~200 $\mu$m. An alternative electrode positioner with a hydraulic system allowed four microelectrodes to be moved independently; this facilitated locating neurons on separate electrodes at the same time. Relative depth differences between these electrodes did not exceed 500 $\mu$m. In some experiments, the four electrodes were arranged in a lateral-medial line to facilitate recording from different layers within a single column. In other configurations, the four electrodes were arranged as close as possible to each other in a square-shaped configuration. Action potentials are discriminated by custom created software (Ohzawa et al. 1996) and time stamped with 40-$\mu$s resolution.

### *Recording procedures*

The recording procedures are identical to those of the preceding companion paper (Menz and Freeman 2004).

### *RF mapping*

For most pairs, dichoptic one-dimensional binary m-sequence noise is used to map RFs (Anzai et al. 1999a,b). For some pairs, a sparse noise stimulus is used, and sometimes both methods are employed. Sixteen adjacent bars are presented for each eye at the mean optimal orientation of multiple neurons for a given eye as illustrated in Fig. 1*A*. The width of the bars is approximately one-fourth the period of the (mean) optimal frequency. The length of the bar is equal to 16 times the width. This square pattern is centered over the (mean) RF center. Computationally, each spike train is cross-correlated with the stimulus sequence by means of the fast m-transform (Sutter 1991) to obtain space-time RF maps for dense noise. Conceptually, a spike train is cross-correlated at a specific time delay with the stimulus sequence at each spatial position to obtain a RF map at that time delay as depicted in Fig. 1*B*. This is repeated for all time delays of interest (0–200 ms) in increments of 5 ms to obtain a space-time RF. The binocular view field is a representation of the stimuli in the axial plane (i.e., the plane defined by the visual axes) assuming a nonhorizontal stimulus orientation (i.e., there can be no horizontal disparity, that encodes stereoscopic depth, if the orientation is horizontal). In Fig. 1*A*, when the luminance polarity of the bars is the same, that position is marked in white. Opposite polarity bar combinations are shown in black. A nonlinear binocular interaction map is obtained by cross-correlating the spike train with each spatial location in the binocular view field pattern. In the maps shown in Fig. 1, *C* and *D*, the white and dark regions indicate excitatory responses to same polarity and opposite polarity bars, respectively.

Sparse noise RF maps are also constructed by cross-correlating the spike train with the stimulus sequence at each spatial location (DeAngelis et al. 1993a,b; Ohzawa et al. 1997). Our sparse noise pattern is tertiary. There are three luminance levels at each spatial position: bright, dark, and gray. For the binocular interaction map, cross-correlation with sparse noise generates four separate maps for each luminance combination bright-bright (BB), bright-dark (BD), dark-bright (DB), dark-dark (DD). To make comparable sparse and deuse noise maps, we generate a composite map from sparse noise as follows: BB+DD-DB-BD.

### *Data analysis*

The two-dimensional binocular interaction maps are reduced to one-dimensional disparity-tuning data by integrating along lines of equal disparity (Ohzawa et al. 1997) as illustrated in Fig. 1, *C* and *D*. The optimal time delay is defined as the correlation delay that produces the largest root mean square signal strength in the one-dimensional tuning data. For this study, only the disparity tuning curves at the optimal delay are considered. The noise of the RF measurement is estimated from the average root mean square of noncausal time slices.

The similarity index (i.e., Pearson product-moment correlation) is a model-free measure of the similarity of a pair of disparity tuning curves

$$\mathrm{SI} = \frac{\sum_{i=1}^{n}(x_i - \bar{x})(y_i - \bar{y})}{\left(\sqrt{\sum_{i=1}^{n}(x_i - \bar{x})^2}\right)\left(\sqrt{\sum_{i=1}^{n}(y_i - \bar{y})^2}\right)} \quad (1)$$

where $x_i$ are the data from one cell at location $_i$, and $y_i$ are the data from the other cell at location $_i$, and $\bar{x}$, $\bar{y}$ are the mean values. The disparity tuning curves are fit with a Gabor function by the Levenberg-Marquardt algorithm (Press et al. 1992)

$$D(d) = \exp(-(d - d_o)^2/2\sigma_d^2)\cos(2\pi f_d(d - d_o) + \phi_d) \quad (2)$$

where $d$ is disparity, $d_o$ is the center position disparity, $\sigma_d$ is the disparity range or size parameter along the disparity axis, $f_d$ is the disparity frequency, $\phi_d$ is the disparity phase. Differences in some parameters (e.g., frequency and size, but not phase) between pairs of cells are normalized by the average value. The quality of the fit is evaluated with the rms of the error. The ratio of signal strength to model error must exceed 1.6 for both cells of the pair to be included in this study. This is an arbitrary value used to indicate reliable signals and determined from observations of all the data. If there are multiple repetitions, the results from the run that produces the strongest signal to noise ratio is used.

Raw neural cross-correlograms are computed between disparity-tuned pairs of cells for all stimulus runs that have at least two repetitions and 1,000 spikes per cell; this includes orientation and spatial frequency tuning runs with sinusoidal gratings and dense and sparse noise stimuli. All raw neural correlograms are shuffle-subtracted to eliminate stimulus-based correlations (Perkel et al. 1967b).

The following steps are used. First, a cross-correlogram is computed using all repetitions, so this includes both stimulus and neural based correlations. Second, the responses from the two cell types are cross-correlated across different repetitions, so this includes only stimulus based correlations and it excludes those that are neurally based. Third, these "shuffled" correlations are subtracted from the first step, yielding neurally based correlations only.

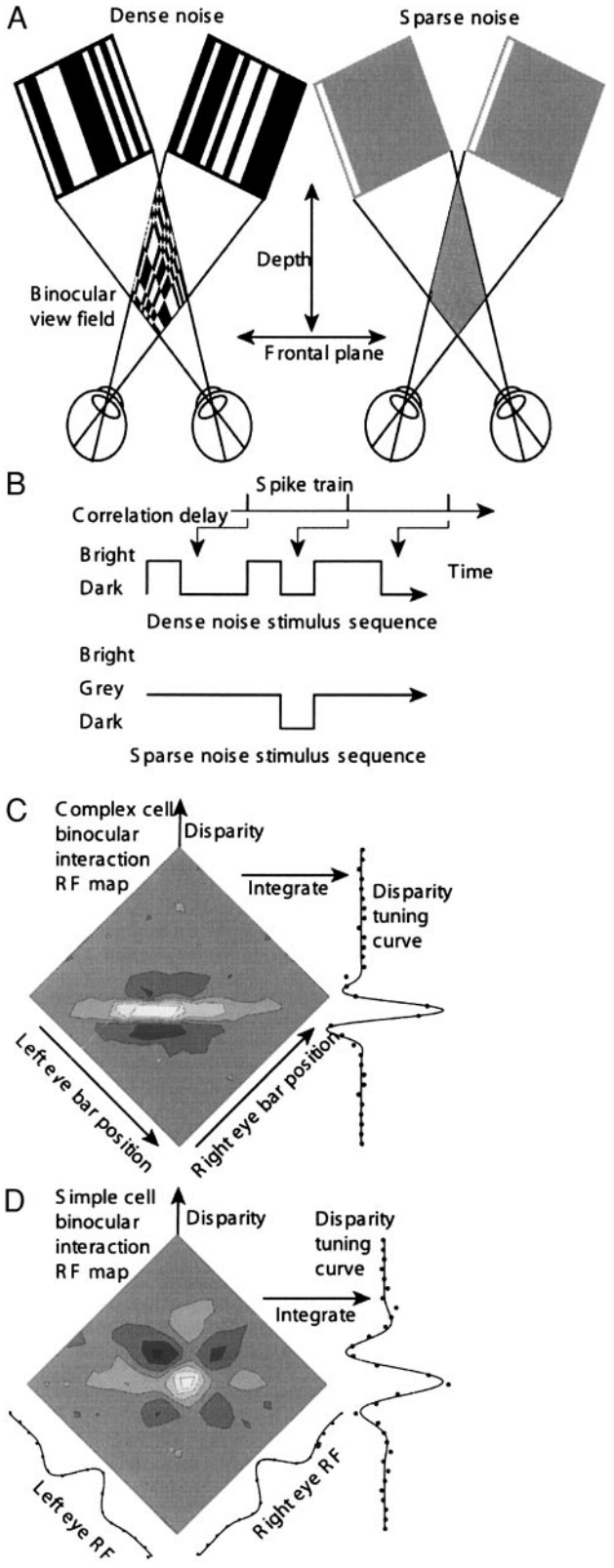


The neural cross-correlogram is binned in increments of 0.5 ms and computed from ±100 ms (the figures only display ±50 ms). Amplitude is normalized by $\sqrt{N_1 N_2}$, and multiplied by 100 to give percentage, where $N_1$ is the number of spikes from cell 1, and $N_2$ is the number of spikes from cell 2 (Brosch and Schreiner 1999). We compute a correlogram asymmetry index, which is a measure of how much the correlogram peak area is shifted from zero (Alonso and Martinez 1998): $\mathrm{AI} = (R - L)/(R + L)$, where $R$ and $L$ are the area of the bins to the right and left of zero, respectively. The cross-correlogram is smoothed with a five-bin Gaussian function. If the pair of cells is recorded from the same electrode, there is a small region around zero correlation (≤ ±2.5 ms) where the two spikes cannot be discriminated. This region is identified and excluded from analysis (exclusion zone). We compute the mean and SD of the shuffled cross-correlogram in the region between ±50 and 100 ms. If the amplitude of a bin exceeds the mean by 3 SDs, then it is considered statistically significant. Cross-correlograms with no significant bins in the range of ±20 ms are excluded from this study.

Multiple significant bins occur adjacent to each other to create an excitatory "peak" in the cross-correlogram. The latency of this peak is at the bin of maximum amplitude. The width of the peak is defined as the width at half-maximum amplitude. The strength of cross-correlation is the area of the peak between half-heights of maximum amplitude (i.e., width). For correlograms measured from the same electrode, sometimes the peak extends across the small exclusion zone ~0 ms, in which case, the estimates of width and strength continue across the exclusion zone. Because of the presence of the exclusion zone, the magnitude of strength and width is underestimated when recordings are from the same electrode. There is no interpolation across the exclusion zone. For any pair of cells, there are multiple cross-correlograms based on the different stimulus runs. The run that produces the greatest cross-correlation strength defines the strength, width, and latency for that pair.

Quantitative criteria are used to distinguish between the different connection types. Monosynaptic connections are defined as having a peak latency ≤3.5 ms, width ≤5 ms, and asymmetry index ≥0.2. Polysynaptic connections are defined as nonmonosynaptic connections having a peak latency ≤10 ms and asymmetry index ≥0.2. Common input connections are defined as having a peak latency ≤5 ms and asymmetry index <0.2 (Menz and Freeman 2003). These quantitative criteria are consistent with known properties of monosynaptic, polysynaptic, and common input connections (Moore et al. 1970). Note that these are mutually exclusive categories, and a cross-correlogram that does not fall into any of these is excluded from this study. After classification, mono- and polysynaptic cross-correlograms are renormalized by the number of presynaptic spikes (i.e., "effectiveness") (Aertsen and Gerstein 1985) and multiplied by 100 to give percentage.

FIG. 1. Dense and sparse noise methods for obtaining disparity tuning curves. *A*: dichoptic binary m-sequence dense noise stimulus consists of 16 bars presented at optimal orientation for each eye, whereas sparse noise has only 1 bar per eye. The binocular view field is a representation of the binocular combination of stimuli, with either bright bars or dark bars in both eyes (same contrast: white), or a bright bar in 1 eye and a dark bar in the other eye (opposite contrast: black), presented at various depths across a fronto-parallel plane. *B*: the spike train is cross-correlated to the binocular combination of stimuli at various delays to obtain a nonlinear binocular interaction map at each correlation delay. *C*: an example of a binocular interaction map for a complex cell at the optimal time delay (i.e., strongest signal). This map illustrates the response of the cell to the same contrast bars presented for each eye (white) or opposite contrast bars for each eye (black) presented at various depths along a fronto-parallel plane. A disparity tuning curve that is fit with a Gabor is obtained by integrating along lines of constant disparity. *D*: this is an example of a simple cell binocular interaction map and the resulting disparity tuning curve.

For the population data, robust regression (Li 1985) is used frequently to quantify correlation between parameters. This technique gives lower weight to data with large residual error and calculates the regression iteratively. It is a quantitative method for reducing the influence of outliers.

## RESULTS

A total of 87 pairs of cells were recorded simultaneously that exhibited binocular interaction maps with signal-to-noise ratios sufficient to reliably extract Gabor parameters. Of these 87 pairs, 59 pairs had statistically significant structure in their neural cross-correlograms, and these pairs are included in this study. Nearly all these paired recordings were derived from two cortical cells. However, in one instance, we recorded four cells simultaneously and obtained five separate pairs. In other multiple cell recordings, we monitored three cells and obtained three pairs in one case and two in another. All cells in this study are disparity tuned and have structure in the resulting neural cross-correlograms that we classify as monosynaptic, polysynaptic, or common input according to the quantitative criteria described in the preceding text (see METHODS). Before presenting data in these categories, it is important to point out that the divisions of connectivity types are somewhat arbitrary. The original designations of these categories were developed from classical studies of neural cross-correlograms based on solid experimental results (Aertsen and Gerstein 1985; Moore et al. 1970; Perkel et al. 1967a,b). These categories are discrete, but there is almost certainly a continuum between them. Even so, the classifications are useful because they reveal correlations between parameters within subpopulations. For the results we present here, the terms "monosynaptic," "polysynaptic," or "common input" connections mean that the correlated firing patterns are consistent with or suggestive of a particular type of connectivity.

Figure 2 shows the distribution of neural cross-correlograms according to their latency, width, and asymmetry index. Cross-correlograms that are consistent with monosynaptic connections have very small latencies and widths but a large value of the asymmetry index (indicating that 1 neuron consistently fires before the other). Connections that could be polysynaptic are also highly asymmetric, but their widths and latencies are generally larger. Pairs of cells that receive some common input are likely to have relatively symmetrical peaks with small latencies but widths may vary.

The cell pairs consist of combinations of simple and complex types as defined by classical criteria (Hubel and Wiesel 1962) and by the predominance of first harmonic or mean firing rates (Mechler and Ringach 2002; Skottun et al. 1991). In Fig. 3, a summary is presented of the various types of connections of the cell pairs analyzed in this study. There are 14 monosynaptic connections, 12 of which are for same electrode recordings. There are 14 polysynaptic recordings, 10 of which are from same electrode recordings. Common input is the most common type of connection (31 pairs). Pairs in Fig. 3 are designated according to electrode spacing for each category. As the data show, the most common pair type is complex-to-complex cell. The least common is complex-to-simple.

### *Binocular energy model*

The motion energy model (Adelson and Bergen 1985; Watson and Ahumada 1985) and binocular energy model (Ohzawa et al. 1990) describe specific characteristics of subunits of complex cells. These subunits have properties that match the RF properties of simple cells (Anzai et al. 1999b,c). If simple cells are the subunits, then one might expect monosynaptic connections from simple-to-complex cells when the simple cell has the same disparity tuning curve as the complex cell and their binocular interaction maps overlap. Previous work has established that there are direct connections from

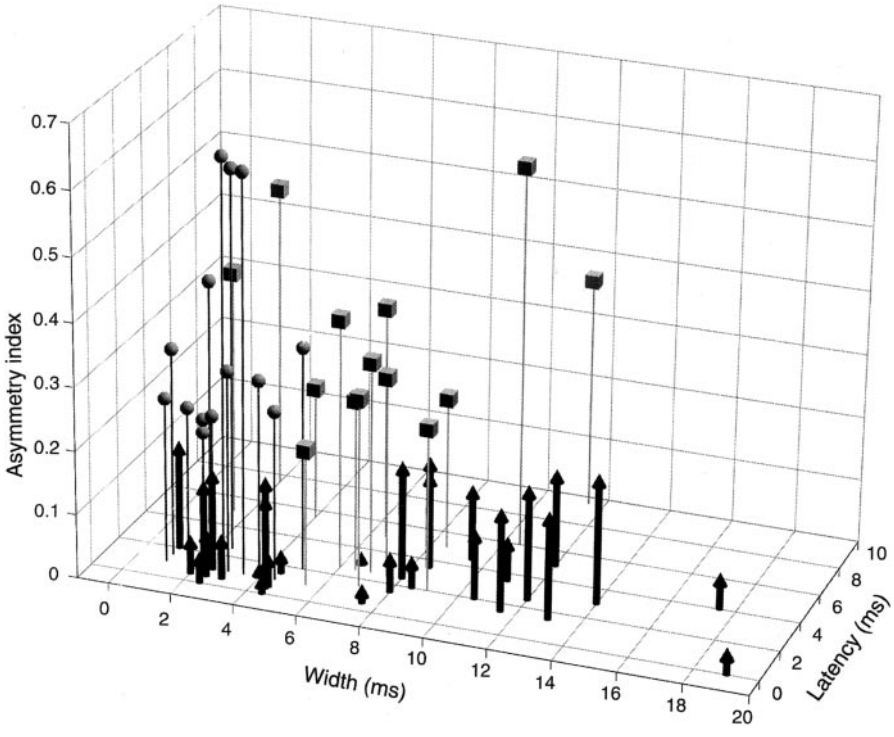


FIG. 2. This 3-dimensional (3-D) scatterplot shows the entire population of neural cross-correlograms plotted in the parameter space that is used to characterize the different types. The peak of the cross-correlogram has a width, latency, and asymmetry index (where 0.0 represents a symmetrical distribution around 0 time delay and 1.0 is maximally asymmetric). Cross-correlograms have characteristics that are consistent with monosynaptic (cube, gray vertical line), polysynaptic (white sphere, white vertical line), or common input (black sphere, black vertical line) types of connectivity. The vertical lines connect each data point to the *x-y* plane making it easier to identify their location in 3-D space.

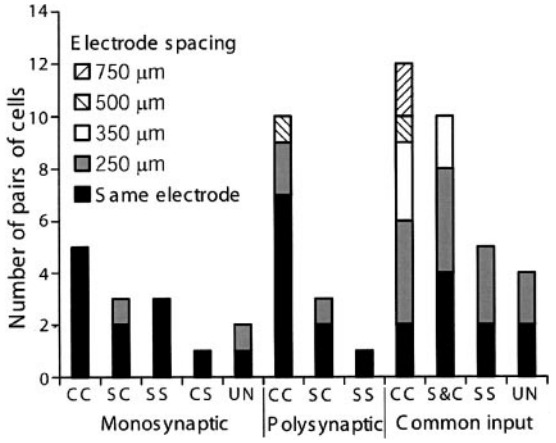


FIG. 3. Population summary by electrode spacing, synaptic type, and cell type. The electrode spacing refers to the lateral distance between the electrodes for a pair of recorded cells. It is the minimum distance possible between the electrode tips for that pair of cells. The criteria used for the classification of synaptic types (e.g., monosynaptic, polysynaptic, and common input) is discussed in METHODS. Neural cross-correlograms that cannot be classified into 1 of these 3 categories is excluded from further analysis. For mono- and polysynaptic connections, there are 4 possible cell combinations: complex to complex (CC), simple to complex (SC), simple to simple (SS), and complex to simple (CS). The unclassified category (UN) is for pairs in which 1 of the cells cannot clearly be classified as simple or complex based on the ratio of the fundamental to DC during a sine wave grating run. These pairs are included in the results. For common input connections there are only 3 types: pairs of complex cells (CC), 1 simple and 1 complex (S&C), and 2 simple cells (SS). Mono- and polysynaptic connections come from the same electrode with just a few exceptions. Common input connections generally come from different electrodes. Connections between complex cells are the most common type found. Every type of possible connection is represented, although complex to simple is very rare ($n = 1$, monosynaptic; $n = 0$, polysynaptic).

simple-to-complex cells, but it is not known whether these fulfill the requirements of the energy model (Alonso and Martinez 1998). Our expectation is that pairs of cells that closely match the energy model requirements will exhibit stronger neural cross-correlograms.

What are the requirements of the binocular energy model? The subunits derive their disparity tuning from either a position or a phase shift difference between monocular RFs, or a combination of both mechanisms(Anzai et al. 1999b,c). The monocular RFs are summed linearly, and the summation is followed by a half-squaring nonlinearity process. The subunits differ only in their monocular phase. A minimum of four subunits is required, and they must be in quadrature.

A good example of a simple-to-complex cell monosynaptic connection that closely matches the requirements of the binocular energy model is shown in Fig. 4. The binocular interaction RF maps (Fig. 4, *A* and *B*) have the typical structure of simple and complex cells, and they are centered and overlap extensively. The one-dimensional disparity tuning data are fit with Gabor functions (Fig. 4*C*). The similarity of the disparity tuning is quantified by the similarity index (SI = 0.73, where 1.0 is identical, 0 dissimilar, −1.0 opposite, see METHODS). In

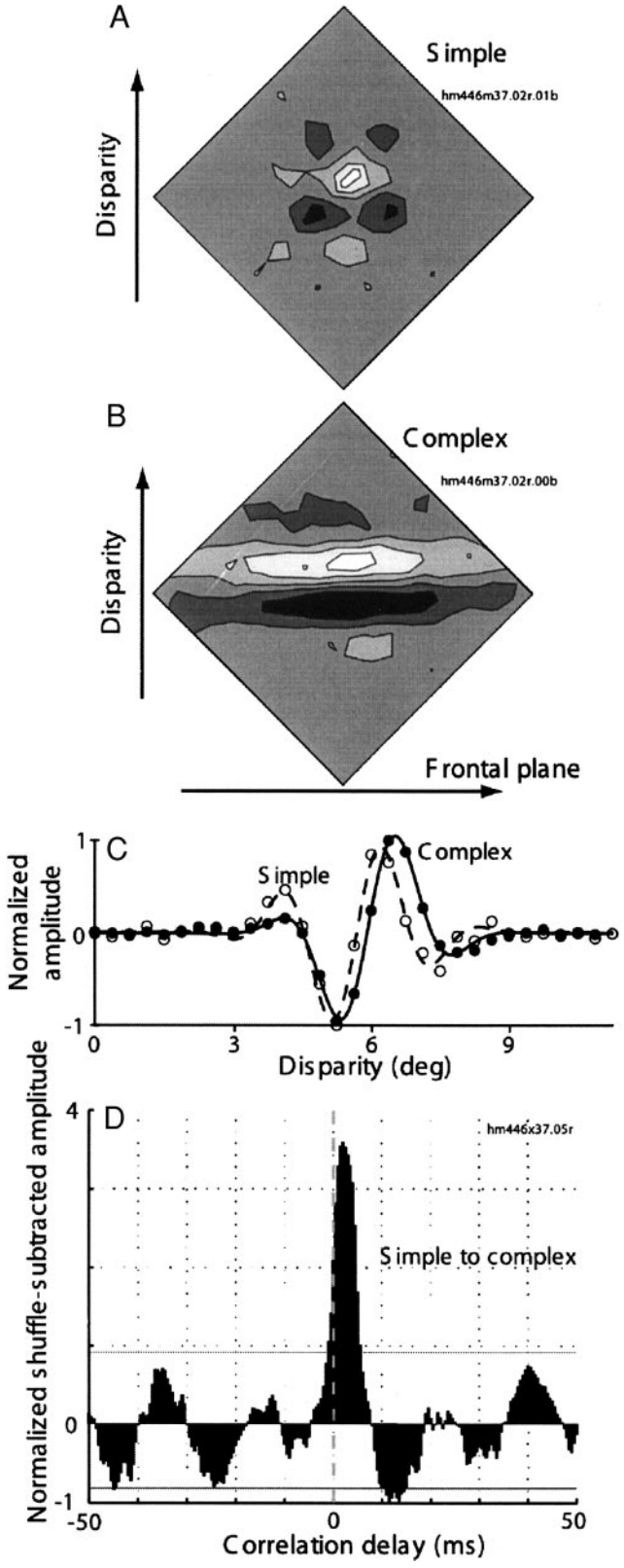


FIG. 4. Binocular energy model example. *A*: binocular interaction map at optimal time delay recorded from a simple cell. *B*: binocular interaction map at optimal time delay for a complex cell recorded simultaneously with *A* from an adjacent electrode (i.e., lateral separation of 250 μm). *C*: disparity tuning curves for the simple cell (open circles, the data, dashed line, the Gabor fit) and complex cell (filled circles, the data; solid line, the Gabor fit) are very similar (similarity index = 0.73). *D*: neural cross-correlogram normalized by the number of presynaptic spikes demonstrates a strong (area of peak = 34.9) monosynaptic peak with the simple cell as the presynaptic cell. Horizontal gray lines, 3 SDs from the mean (evaluated from correlation delays between 50 and 100 ms). Vertical dashed gray line, 0 correlation difference. Both cells were recorded from layer 4. This is an example that is consistent with the binocular energy model.

terms of the Gabor fit, the presynaptic simple cell is 0.08 cycle/° higher in disparity frequency, exhibits a 0.4° position shift and differs in phase by 25°. The negative subregions, which are excitatory to opposite contrast, are highly overlapping. The positive subregions, which are excitatory to same contrast, are shifted a little from the combination of position, phase, and spatial frequency differences. This cell pair is not a perfect fit for the energy model, yet the neural cross-correlogram has a strong peak [strength = 34.9 (see METHODS)] and is classified as monosynaptic (Fig. 4*D*). These cells were recorded from adjacent electrodes in layer 4 with an estimated lateral separation of 250 $\mu$m.

In Fig. 5, we show a pair of cells that clearly do not meet the requirements of the energy model. The binocular interaction maps (Fig. 5, *A* and *B*) look like classic simple and complex cell structures. They are overlapping, but the disparity tuning curves are in nearly perfect quadrature (93° phase difference). The phase of the simple cell is 96°, and the phase of the complex cell is –3°. The similarity index is 0.02. The presynaptic simple cell has a higher spatial frequency (by 0.13 cycle/°) and larger size (range) parameter (by 0.11°). There is a monosynaptic peak in the neural cross-correlogram of reasonable strength (12.6). This pair is recorded in layer 4 from a single electrode, so there is an artifactual blank area near the zero correlation because it is not possible to discriminate two different spikes from the same electrode when the temporal separation is <2.5 ms. Another example in which the pair has similar tuning characteristics is shown in Fig. 6. In this case, there is a unique lack of structure in the cross-correlogram. This example makes the point that similar disparity-tuned pairs do not necessarily show highly correlated firing patterns. As with the previous examples, the binocular interaction maps have typical structure for simple and complex cells. They are overlapping, and disparity tuning is similar (SI = 0.71) even though there is no structure in the neural cross-correlogram. There are two notable differences between this example and the one shown in Fig. 4. The pair in Fig. 4 was located in layer 4. In this example, the simple cell was recorded from layer 2,3 and the complex cell was from layer 4. In Fig. 4, the simple cell had higher disparity frequency content. In this example, the simple cell is lower in disparity frequency compared with the complex cell (by 0.08 cycle/°). As shown below, the difference in disparity frequency is important.

### *Strength versus similarity*

We next examine the relationship between strength of neural cross-correlation and similarity of the pairs in the population. The obvious question is do monosynaptic pairs with similar disparity tuning have stronger neural cross-correlation? Based on previous cross-correlogram studies, pairs of cells with similar RFs tend to have stronger connections (Alonso and Martinez 1998; Brosch and Schreiner 1999; DeAngelis et al. 1999; Reid and Alonso 1995). This question is addressed in Fig. 7

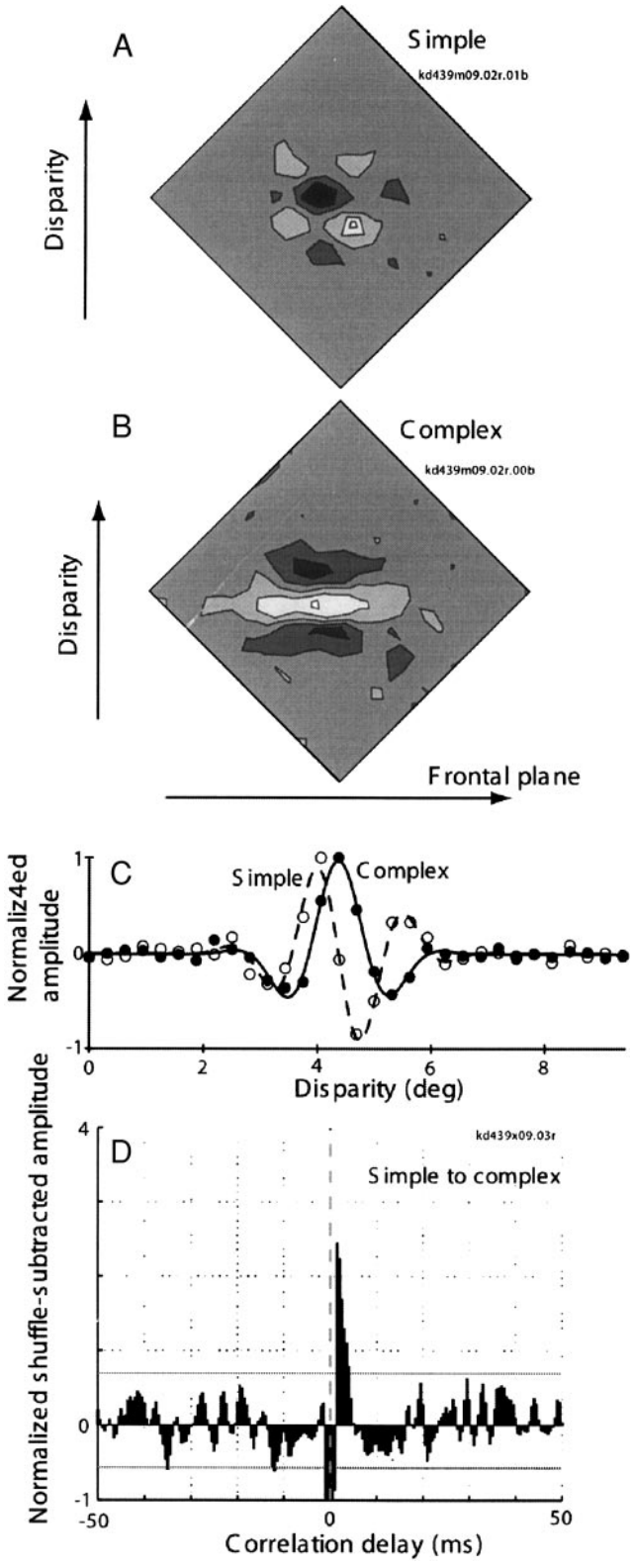


FIG. 5. Simultaneous recording of simple and complex cell. *A*: binocular interaction map at optimal time delay recorded from a simple cell. *B*: binocular interaction map at optimal time delay for a complex cell recorded simultaneously with *A* from the same electrode. *C*: the simple cell (open circles, the data; dashed line, is the Gabor fit) and complex cell (filled circles, the data; solid line, the Gabor fit) have disparity tuning curves that are in nearly perfect quadrature (similarity index = 0.02). This is *not* the quadrature between monocular simple cell receptive fields shown in the binocular energy model (Fig. 4). The binocular energy model would predict either no connection or a very weak connection between cells with such different disparity tuning. *D*: neural cross-correlogram normalized by the number of presynaptic spikes demonstrates a monosynaptic peak (area of peak = 12.6) with the simple cell as the presynaptic cell. Horizontal gray lines, 3 SDs from the mean (evaluated from correlation delays between 50 and 100 ms). Vertical dashed gray line, 0 correlation difference. Both cells were recorded from layer 4.

where the most similar pairs are to the left side of the *x* axis. There are different ways of characterizing similarity of tuning. In Fig. 7*A*, we use our similarity index. There is a group of cells with SI >0.6 (*similar*, ●), and another group with SI <0.05 (*dissimilar*, ○). The large gap between the groups is a natural zone of discrimination because the distribution is bimodal. The similar group has stronger neural cross-correlation values compared with the dissimilar group ($P = 0.039$, Wilcoxon rank-sum test). It is important to note here that there are connections between cells with dissimilar tuning, some of them with nearly opposite tuning profiles, but the strength of these connections tends to be very weak. We should also point out that we first made a general comparison for the entire population of cells without reference to categories of monosynaptic, polysynaptic and common input. There were generally no correlations between parameters of interest. We then used the classification system on a subpopulation to reveal interesting correlations between parameters.

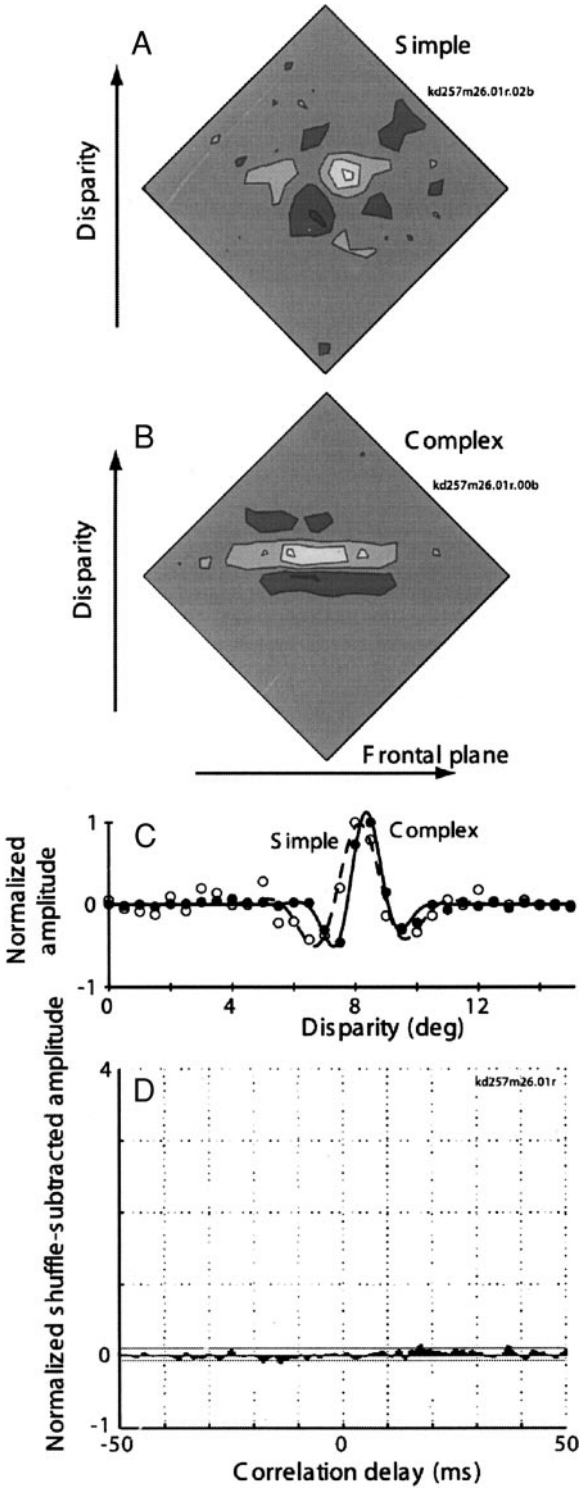


FIG. 6. A simple-complex pair with similar disparity tuning but with a flat cross-correlogram. This is the only data included in the paper with no structure in the cross-correlogram. It demonstrates that not all pairs with similar tuning have structure in their cross-correlogram. *A*: binocular interaction map at optimal time delay recorded from a simple cell. *B*: binocular interaction map at optimal time delay for a complex cell recorded simultaneously with *A* from an adjacent electrode (i.e., lateral separation of 250 $\mu$m). *C*: disparity tuning curves for the simple cell (open circles, the data; dashed line, the Gabor fit) and complex cell (filled circles, the data; solid line, the Gabor fit) are very similar (similarity index = 0.71). *D*: there is no significant structure in the neural cross-correlogram. Horizontal gray lines, 3 SDs from the mean (evaluated from correlation delays between 50 and 100 ms). Vertical dashed gray line, 0 correlation difference. The simple cell was recorded from layers 2,3, whereas the complex cell was in layer 4. The lack of structure in the neural cross-correlogram may be related to the location of the cells.

Phase and frequency are the two Gabor parameters that define the shape of disparity tuning. An alternate measure of similarity is the phase difference in the fitted Gabors (Fig. 7*B*). We have drawn the distinction between similar and dissimilar at a phase difference of 45 because it is near the median value (i.e., 43) and produces the exact same groupings as shown in Fig. 7*A*, so the statistics are the same. The similar pairs in Fig. 7*A* all have a phase difference of <45° in Fig. 7*B*. The pairs with nearly opposite phase tuning have the weakest cross-correlograms (○).

A third measure of similarity is based on spatial frequency difference. The difference in frequency is normalized by the average frequency. The data are split into similar and dissimilar groups at the median value of 22.5%. The similar group has a stronger neural cross-correlogram compared with the dissimilar group with larger frequency differences ($P = 0.025$, Wilcoxon rank-sum test). The tendency for similar disparity-tuned pairs to have stronger neural cross-correlograms only holds for monosynaptic pairs. This relationship is not maintained for polysynaptic and common input connections as determined by the same methods used for the data in Fig. 7. Because binocular disparity tuning is determined by the difference in right and left RFs, it is possible for a pair of cells to have very different disparity-tuning properties but have similar monocular tuning. It is also possible for a pair of cells to have identical disparity tuning and different monocular RFs in the two eyes. If connectivity between neurons is based on dominant-eye monocular RF similarity, that does not necessarily translate into disparity-tuning similarity. It is possible that cells with dissimilar disparity-tuning properties and strong neural cross-correlations are connected together because of dominant-eye monocular RF similarity.

### *Some functional implications*

We must consider the possibility that some of the binocular disparity-tuned cell pairs we have studied may not play a role in stereopsis. They may be signaling some other aspect of the

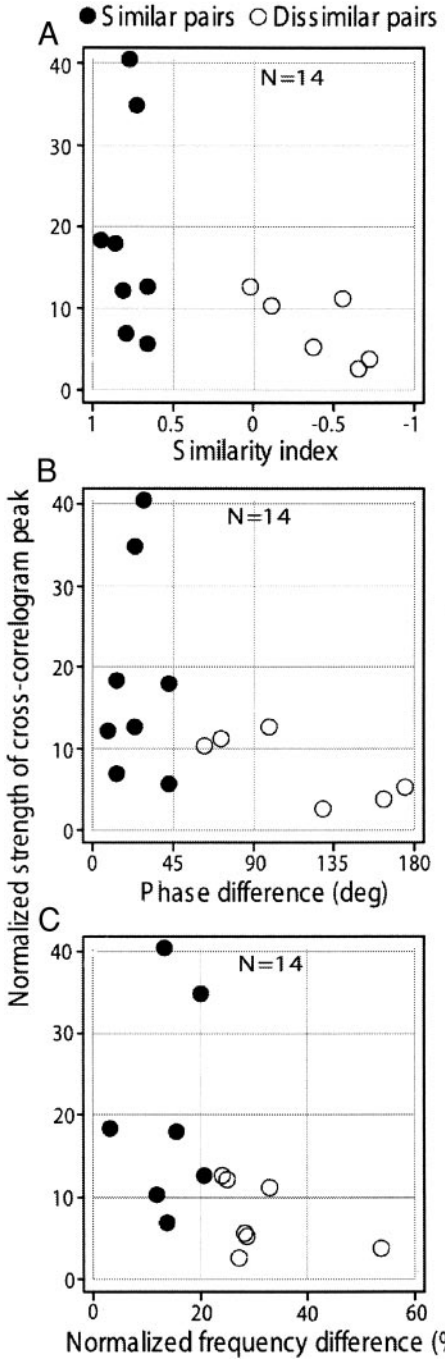


FIG. 7. Monosynaptic neural connections are stronger between pairs of cells with similar disparity tuning. *A*: the normalized strength of the cross-correlogram peak is plotted against the similarity index (SI, as defined in METHODS), where an SI = 1.0 corresponds to identical pairs and SI = –1.0 are exact opposites. There is an absence of cells with an SI between 0.05 and 0.6, so this gap is used to discriminate similar tuning (SI > 0.6, ●) from dissimilar tuning (SI < 0.05, ○). The similar pairs have a stronger cross-correlation peak compared with the dissimilar pairs ($P = 0.039$, Wilcoxon signed-rank). *B*: the difference in Gabor phase between the pairs is an alternate measure of similarity. The pairs with a phase difference of <45° are the exact same pairs with a SI > 0.6. *C*: a 3rd measure of similarity is the difference in frequency normalized by the average frequency. The median value is 22.5%. The data are split into similar and opposite pairs based on the median value. The similar pairs have a stronger cross-correlogram peak ($P = 0.025$, Wilcoxon signed-rank).

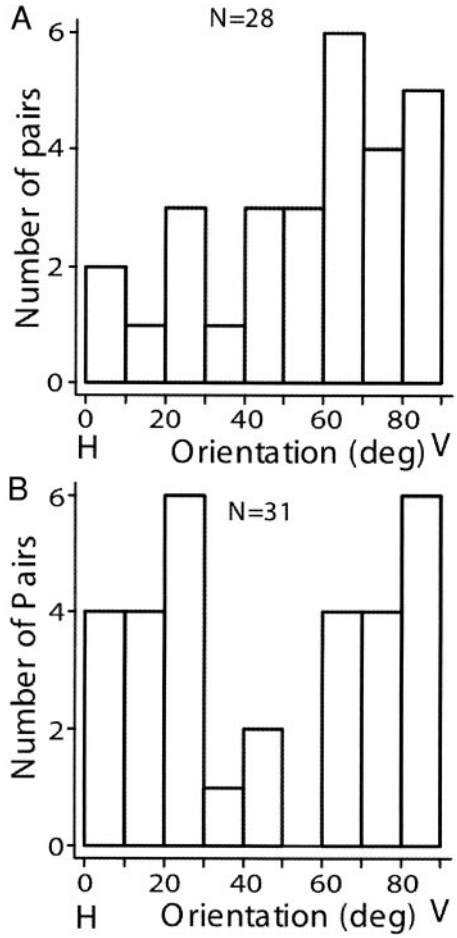


FIG. 8. Distributions of optimal orientations for disparity-tuned pairs. Zero degrees corresponds to horizontal, and 90° is vertical. *A*: the distribution of optimal orientations for all mono- and polysynaptic pairs demonstrate a bias in favor of vertical orientations ($P = 0.023$, $\chi^2$, orientation split into 2 groups) that encode horizontal disparity used in stereopsis. *B*: for common input connections, there is a deficit of oblique orientations ($P = 0.02$, $\chi^2$, orientation split into thirds).

stimulus, such as motion. Stereopsis requires horizontal disparity, which results when cell-orientation preferences are near vertical. Vertical disparity in natural scenes arises from the difference in image size created when objects are closer to one eye. Vertical disparity is useful to the visual system (Backus et al. 1999; Berends and Erkelens 2001), but it is not necessary for the perception of depth through stereopsis. Cell pairs tuned to nearly horizontal orientations (vertical disparities) do not have a direct perceptual role in stereopsis.

The orientation preference distribution of our cell-pair sample is shown in Fig. 8. For mono- and polysynaptic pairs, there is a clear bias in favor of vertical orientations (Fig. 8*A*). More cell pairs are tuned to nearly vertical compared with nearly horizontal orientations. The distribution for common input connections appears to be different (Fig. 8*B*). Horizontal and vertical orientations are equally well represented, but there is a deficit of oblique orientations. This could be related to the *oblique effect*, i.e., human subjects exhibit reduced spatial resolution for visual detail at oblique orientations (Appelle 1972). There are analogous effects in the visual cortex (Li et al. 2003). For mono- and polysynaptic connections, the bias for vertical orientations suggests that these cells could be involved

in stereopsis. For common input cell pairs, about half are not likely to be processing stereopsis because they are tuned to nearly horizontal orientations.

### *One versus two electrodes*

We now consider possible differences between cell pairs recorded from the same electrode versus those for which neurons are recorded from different electrodes. Same electrode pairs are presumed to be physically closer together and might exhibit different RF relationships compared with those from separate electrodes. Pairs of cells involving at least one simple cell have slightly different distributions of similarity index values for same versus different electrode pair samples (Fig. 9). Same electrode pairs (■) can have similar or near quadrature disparity tuning, but it is rare for them to have opposite tuning, i.e., large negative values. A quadrature relation is one in which all parameters are equal except phase, which is 90° different. Near quadrature tuning has a similarity index near zero. In terms of similarity index values, the simple and complex cells shown in Fig. 5 and 6, respectively, may be categorized as similar or quadrature types. The pairs recorded from different electrodes (Fig. 9, □) tend to lack quadrature (only 1 pair with a near 0 SI), are more often nearly opposite and also more frequently have similar disparity tuning. There are reports that pairs of adjacent simple cells have monocular RFs in quadrature (Liu et al. 1992; Pollen and Ronner 1981), but other work establishes that many phase relationships exist between cell pairs. (DeAngelis et al. 1999). A recent report suggests a bias for odd and even symmetric spatial phase in visual cortex (Ringach 2002).

### *Complex-to-complex cells*

The most common type of cell pair in our sample is between complex cells ($n = 27$). There is a sufficient number of these pairs to make some generalizations about connections between disparity-tuned complex cells. A representative sampling of complex-to-complex mono- and polysynaptic pairs of disparity-tuned cells is shown in Fig. 10. An example of an oppositely tuned monosynaptic pair is shown in Fig. 10*A*. This pair has a similarity index of −0.72 due to the obvious phase difference (164°). There is also a difference in spatial frequency of 0.15 cycle/° in which the presynaptic cell (spike 1) has the higher value. A polysynaptic example is shown in Fig. 10*B*. This pair has a phase difference of 91°, but no quadrature because of other differences in their parameters. The presynaptic cell has the higher spatial frequency (by 0.11 cycle/°). There is also a position difference; the presynaptic cell is shifted to the right by 0.3°. The combination of this position shift and higher spatial frequency content moves the location of the optimal disparity closer to that of the postsynaptic cell (i.e., the positive peaks nearly coincide, in spite of the 90° phase difference). We would expect a similarity index of 0.0 for a 90° phase shift, but because of the shift in the optimal disparity due to spatial frequency and position differences, the similarity index is 0.58. In Fig. 11*C*, the presynaptic cell (spike 1) has a higher spatial frequency (by 0.08 cycle/°) and a fairly large position shift of 0.8°, which results in alignment of the negative peaks. A negative peak is excitatory to opposite contrast visual stimulation, and we assume that same contrast stimulation causes suppression. As a result of this alignment of negative peaks, the similarity index is 0.66, which is indicative of a fairly similar pair. In all of the examples presented so far, the presynaptic cell has a higher disparity frequency. In Fig. 10*D*, we present an example in which the presynaptic cell (spike 2) has a slightly lower disparity frequency by (0.04 cycle/°) and a much larger size parameter (0.8°). The cross-correlograms in Fig. 10 are all plotted on the same scale to facilitate amplitude of the correlation strength comparisons. The example in Fig. 10*D* has a much stronger correlogram peak compared with the other examples shown. We observed a wide variety of differences in the fitted Gabor parameters: phase, position, disparity frequency, and size. Nonetheless, pairs tend to be either similar or opposite in tuning based on similarity index. They are different in ways that tend to bring the peaks or troughs into alignment.

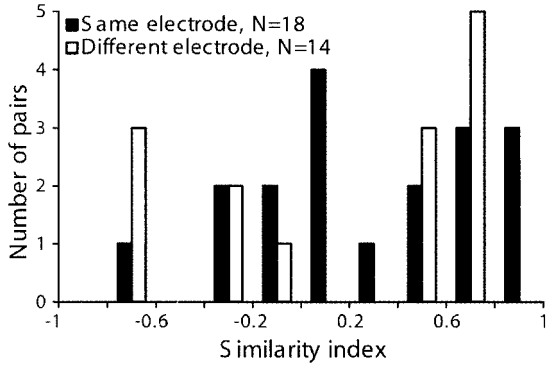


FIG. 9. Distribution of SI involving ≥1 simple cell. The distribution is split between pairs measured to the same electrode (■, presumed to be physically close) and pairs recorded between different electrodes (□, cells that are further away from each other). Same electrode pairs tend to have either similar tuning (SI ≅ 1) or near quadrature tuning (SI ≅ 0), with only 1 pair having nearly opposite tuning (SI ≅ −1). For more distant pairs, there is still a group with similar tuning, but there is a relative absence of quadrature pairs and more opposite pairs.

We expect the distribution of similarity indices to have a bias in favor of similar pairs because of the physical proximity of many pairs and the prevalence of monosynaptic connections. The actual distribution for all complex-to-complex cell pairs is surprising (Fig. 11*A*). There is a clearly bimodal distribution in which pairs can be classified as similar or opposite in tuning. The distribution is well fit by two Gaussian functions. For common input connections, similar pairs outnumber opposite pairs; but mono- and polysynaptic pairs are equally split between similar and opposite pairs. The large number of opposite pairs is unexpected, and the total absence of near quadrature pairs (SI = ~0) is striking. The strength of the neural cross-correlograms as a function of similarity index is shown in Fig. 11*B*. Our expectation that the opposite pairs will have weak correlograms does not hold. There is no difference in cross-correlogram strength between opposite and similar pairs ($P = 0.92$ Wilcoxon rank-sum). The expectation that cells with similar RFs tend to have stronger neural cross-correlograms is not necessarily borne out.

### *Fine-to-coarse and coarse-to-fine tuning*

In the examples shown in the preceding text, there is a tendency for the presynaptic cell to have a higher disparity frequency compared with the postsynaptic cell. To explore this

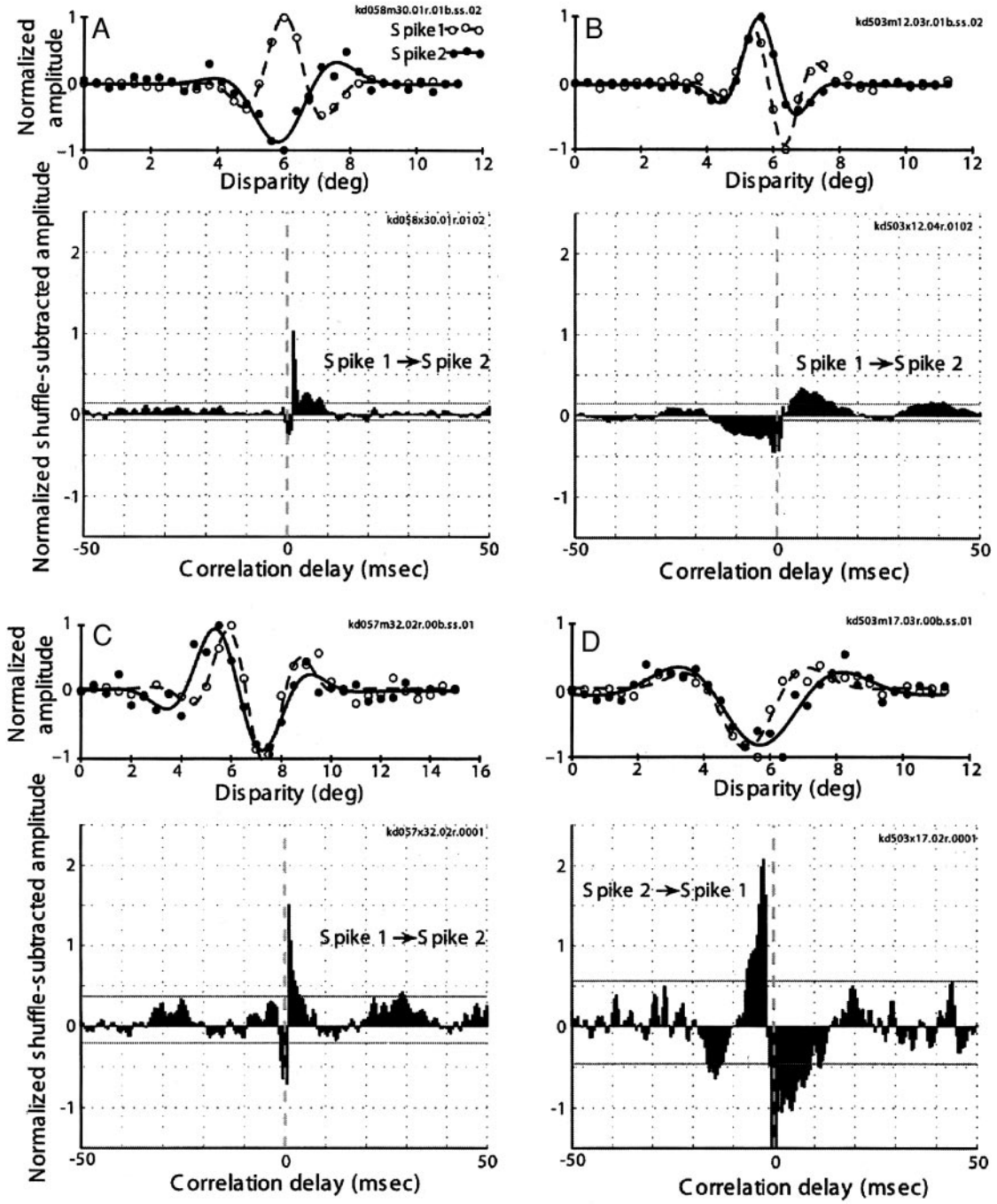


FIG. 10. Examples of mono- and polysynaptic connections between pairs of complex cells. *A*: monosynaptic connection between cells with nearly opposite disparity tuning (SI = −0.72, phase difference of 164°). The presynaptic cell (spike 1) has a higher frequency (0.35 cycle/°) compared with the postsynaptic cell (0.2 cycle/°). *B*: polysynaptic connection between cells with similar disparity tuning (SI = 0.58). The phase difference is 91° for this pair, which means that they would be in quadrature (SI = 0) if the other parameters were equal. However, there is a difference in frequency (presynaptic spike 1 = 0.46 cycle/° and postsynaptic spike 2 = 0.35 cycle/°) and position (presynaptic spike 1 = 6.0° and postsynaptic spike 2 = 5.7°) that brings the optimal disparities close together. *C*: monosynaptic connection between cells with similar disparity tuning (SI = 0.66). This pair has a phase difference of 43°. The presynaptic cell spike 1 has a higher frequency (0.31 cycle/°) compared with the postsynaptic cell spike 2 (0.23 cycle/°). There is a position shift of 0.8°, which has the effect of bringing the opposite contrast excitatory subregions (at 7.25°) in alignment. *D*: monosynaptic connection between cells with similar disparity tuning (SI = 0.66). This pair has a phase difference of only 25°. The presynaptic cell *spike 2* has a lower frequency (0.17 cycle/°) and larger size parameter (2.1°) compared with the postsynaptic cell *spike 1* (0.21 cycle/° and 1.3°). This pair has a stronger peak in the cross-correlogram compared with the other pairs shown (12.5 compared with 3.8, 6.0 and 5.6).

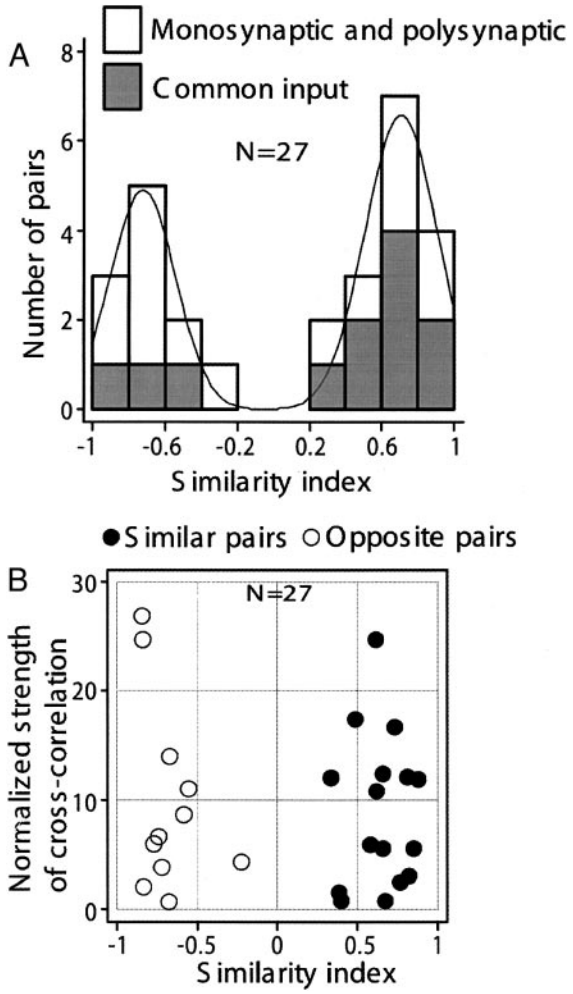


FIG. 11. Complex-complex connections lack quadrature. *A*: distribution of similarity index for complex-complex pairs broken down by mono- and polysynaptic connections (□) and common input connections (▨). There is an obvious deficit of similarity indices around 0, indicating an absence of quadrature pairs. —, a nonlinear fit to the sum of 2 Gaussian functions ($P = 0.0034$, $R^2 = 0.98$). The locations of the peaks are at SI = −0.72 and SI = 0.71. Complex-complex pairs can be described as being either similar or opposite in their disparity tuning. For poly- and monosynaptic connections, there is an even split between similar and opposite pairs. For common input connections, there are 3 times as many similar pairs as opposite pairs. *B*: there is no difference in neural cross-correlation strength between opposite and similarly tuned pairs ($P = 0.92$, Wilcoxon signed-rank).

more completely, a population summary for all mono- and polysynaptic connections is given in Fig. 12*A*. This is a histogram of the normalized disparity frequency difference in which HF and LF refer to high and low frequency, respectively. As the histogram shows, most of the data fall to the left of zero, indicating that the presynaptic cell has the higher disparity frequency ($P = 0.006$, sign test). The mean frequency difference is 12.3%, but there are a few pairs of cells with large frequency differences. We expect disparity range (size) to be correlated to disparity frequency; higher frequency cells should have smaller RFs. This implies that the disparity range of the presynaptic cell should be smaller compared with that of the postsynaptic neuron. The anticipated relationship is confirmed in Fig. 12*B*, although there is not as strong an effect as that for frequency ($P = 0.028$, sign test). This is consistent with the observation that the correlation between spatial frequency and size is affected by the fact that higher frequency cells tend to have more subregions (DeAngelis et al. 1995).

A central finding of this study is illustrated in Fig. 12*C*. When the presynaptic cell has a larger disparity range, it tends to have a stronger neural cross-correlogram (data to the left of the vertical dashed line). The strength of cross-correlation is $\geq 10$ for nearly all coarse-to-fine pairs, and the values are much lower for smaller disparity range presynaptic cells (to the right of 0, fine-to-coarse). Figure 12*D* shows a disparity frequency-size correlation, which applies to complex-to-complex cell connections. When the presynaptic cell is higher in disparity frequency, it also tends to be smaller in disparity range (size). There is a spatial frequency-size correlation for complex–to-complex cell combinations. In summary, there are more pairs in which the presynaptic cell has higher spatial frequency (a fine-to-coarse system). Connection strength is stronger when the presynaptic cell is larger in size (a coarse-to-fine system). Considered together, these findings suggest that there are both coarse-to-fine and fine-to-coarse processes at work. A postsynaptic cell that pools across neurons of different spatial frequency content receives a weighted average of its inputs. This configuration contains pairs of both coarse-to-fine and fine-to-coarse cell combinations. The system may function as follows. Pooling over neurons that share a similar peak or trough in their disparity tuning curves (see Fig. 12, *B–D*) but vary across disparity scale (i.e., different disparity frequency and disparity range) will disambiguate the true disparity and reduce false matches (Fleet et al. 1996). Coarse disparity scale information is processed more quickly (Menz and Freeman 2004). When this is combined with stronger coarse-to-fine connections, it may establish a bias for coarse information to constrain the perceived disparity.

## DISCUSSION

In the experiments reported here, we have conducted electrophysiological studies of pairs of disparity-tuned cortical neurons that were recorded simultaneously using different electrode configurations. Cross-correlogram analysis was carried out for the recorded cell pairs. Pairs were identified that exhibit excitatory monosynaptic, polysynaptic, or common input types of structure in their neural cross-correlograms. Monosynaptic pairs, which almost always come from the same electrode, tend to have stronger cross-correlogram peaks when their disparity tuning is similar. We find simple-to-complex cell monosynaptic connections that are consistent with the binocular energy model, but the sample size is relatively limited.

Vertical orientation encodes horizontal disparity that is necessary for stereopsis. We find that for mono- and polysynaptic connections there is a bias for vertical orientations, implying that these pairs are playing a role in stereopsis. For common input connections, there is an oblique effect, a deficit of pairs tuned to oblique orientations, and an equal quantity of horizontal and vertical orientations. Even though all pairs are tuned to binocular disparity, the common input pairs may be playing a different functional role.

### *Cell-pair tuning relationships*

Most previous studies of cortical cell cross-correlations support the idea that neurons with similar RF locations tend to

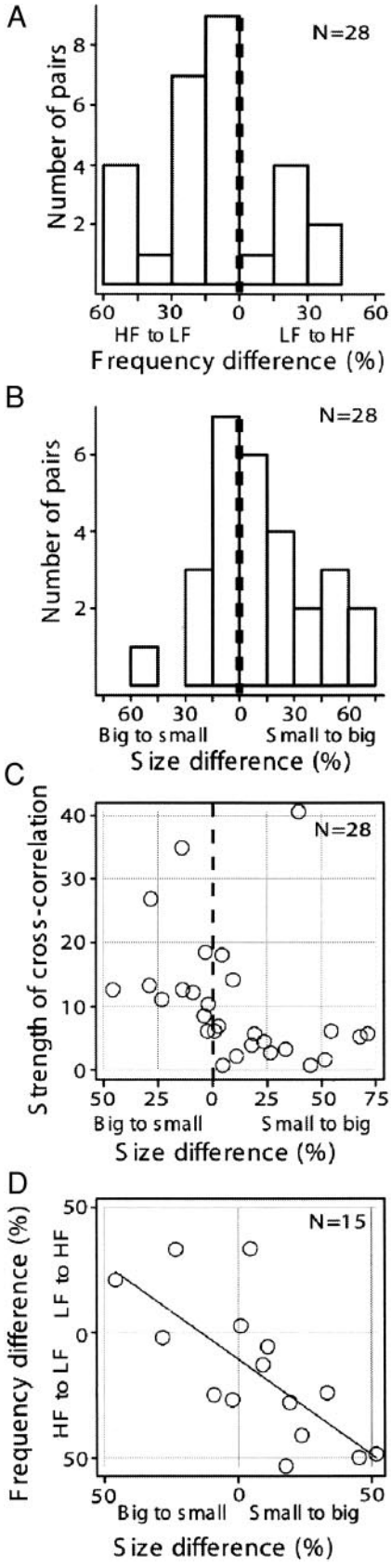


have stronger connections (Alonso and Martinez 1998; Arnett and Spraker 1981; Brosch and Schreiner 1999; DeAngelis et al. 1999; Ghose et al. 1994b; Hata et al. 1991; Kruger and Aiple 1988; Nelson et al. 1992; Reid and Alonso 1995; Schwarz and Bolz 1991; Tanaka 1983). One report suggests that the strength of cross-correlations depends only on lateral cortical distance and is independent of orientation (Das and Gilbert 1999). This result is at odds with all other findings that indicate stronger connections between similar orientation pairs. Our monosynaptic results are consistent with the general trend of stronger connections between similar pairs. We also find a correlation between disparity-tuning similarity and cross-correlation strength, as described in the preceding text.

Some previous reports indicate that adjacent simple cells are either in quadrature (90 degree phase difference) or anti-phase (180 degree phase difference) (Liu et al. 1992; Pollen and Ronner 1981). Their quadrature pairs (13/16, 83–105° difference as shown previously) (Liu et al. 1992) generally had no structure in their neural cross-correlogram, whereas the anti-phase pairs (3/16, 160–194° difference) exhibited mutual inhibition. No excitatory connections were found, and one common input connection was reported between adjacent simple cells. Other results of recordings from pairs of adjacent simple cells have shown mono- and polysynaptic excitation and common input connections (DeAngelis et al. 1999; Ghose et al. 1994a). The phase differences between pairs that were otherwise similar consisted of all values including 90 and 180° (9/12 are between 120 and 180°, 2 pairs are $<30°$, and only 1 pair is between 90 and 120°) (DeAngelis et al. 1999). This distribution is clearly not consistent with the quadrature/anti-phase distribution described previously (Liu et al. 1992). However, the distribution of spatial phase in visual cortex appears to be biased toward even and odd symmetry, which would favor quadrature pairing for connected cells (Ringach 2002). In our current study, the sample size for simple-to-simple connections from the same electrode is very small ($n = 6$). Nonetheless, we still find all types of neural cross-correlograms: monosynaptic, polysynaptic, and common input.

Disparity quadrature is very different from monocular RF quadrature. Disparity tuning is determined by the relationship between left and right eye RFs. If responses of a pair of cells show quadrature for both left and right eye RFs, their disparity tuning is the same (binocular energy model subunits). Similar disparity tuning does not imply similar monocular RF tuning. It means that there is a similar relationship between left and

FIG. 12. Frequency and size relationships of mono- and polysynaptic pairs. *A*: the distribution of the difference in frequency between the pairs normalized by the average frequency of the pair. To the left of - - -, the presynaptic cell has a higher frequency, whereas to the right, the presynaptic cell has a lower frequency. The dominant direction is from higher to lower frequency ($P = 0.0063$, sign test). *B*: the distribution of the difference in size between the pairs normalized by the average size of the pair. To the left of - - -, the presynaptic cell has a larger size, whereas to the right, the presynaptic cell has a smaller size. The dominant direction is from smaller size to larger size ($P = 0.028$, sign test). *C*: the strength of the neural cross-correlation as a function of the size difference shown in *B*. When the presynaptic cell is larger in size, the cross-correlation tends to be stronger ($P = 0.0028$, Wilcoxon signed-rank). *D*: for complex-to-complex cells only, there is a disparity-frequency disparity range (size) correlation. The change in frequency is plotted against the change in size. When the presynaptic cell is lower in frequency, it also tends to be larger in size compared with the postsynaptic cell. Conversely, if the presynaptic cell is higher in frequency, then it also tends to be smaller in size compared with the postsynaptic cell (robust regression, $P = 0.003$).

right eye RFs. If a pair of cells have one eye's RFs in quadrature but the other eye's RFs have the same (or opposite) tuning, that will produce quadrature in disparity tuning. If there were only quadrature and anti-phase monocular relationships, that limits the possible disparity relationships to similar tuning and quadrature tuning. If we expand our sample to include connections between simple and complex, in addition to simple with simple, then we have a reasonable sample size ($n = 18$ for same electrode, $n = 14$ for different electrode, Fig. 9). We find that for same electrode pairs the distribution includes both similar tuning and near quadrature tuning. There are other ways of generating this kind of distribution besides quadrature/anti-phase monocular RFs, but the data are consistent with that hypothesis. The distribution for pairs from different electrodes appears to lack quadrature. This also supports the hypothesis that there is a special quadrature relationship between nearby cells. Quadrature disparity tuning relationships among physically nearby simple cells may be more common than monocular RF quadrature. The three binocular simple cell examples shown previously (DeAngelis et al. 1999) are in near quadrature (i.e., similarity indices close to zero) for their disparity tuning but not in their monocular RFs.

Our pairs of complex cells tend to have either similar or opposite tuning with an obvious lack of quadrature. The main peaks and troughs in the disparity tuning curves tend to be aligned, which creates the biphasic distribution. It is not the case that the phase difference is always 0 or 180° with the other parameters being equal. The distribution includes all three types of neural cross-correlations.

Monocular quadrature and similarity of disparity tuning is the basis for the binocular energy model, but what function is served by disparity quadrature and opposite disparity tuning? If a cell pools over disparity-tuned subunits in quadrature followed by a half-squaring nonlinearity, then the postsynaptic cell will respond to all disparities just as a complex cell responds to all monocular phases. We find some complex cells that are clearly binocular but are not disparity selective. They may be the same population of complex cells that does not exhibit phase-specific binocular interaction to dichoptically presented gratings (Ohzawa and Freeman 1986). This disparity-energy model consists of subunits in which some pairs have opposite disparity tuning, whereas other pairs have quadrature disparity tuning. This potentially explains the presence of quadrature and opposite pairs but not why the subunits are connected to each other in an excitatory manner. It could be that this connectivity is based on monocular relationships. The energy model may represent a cortical building block replicated at higher levels of signal processing.

### *Spatial pooling*

To solve the global stereo correspondence problem it is desirable to combine information across spatial scale (Marr and Poggio 1979). Low-frequency cells can respond to a large range of disparities but with poor resolution. High-frequency neurons have good resolution but limited range. The original idea was that the solution at coarse scales would shift (with or without eye movement) the range of high-frequency neurons. This particular implementation of coarse-to-fine called "shifting" is not likely to occur (Rohaly and Wilson 1993; Smallman and MacLeod 1997). However, the basic and appealing notion, developed in the preceding paper (Menz and Freeman 2004) is that a coarse-to-fine mechanism operates such that a solution at a coarse spatial scale occurs more quickly and constrains one at higher frequencies. The current study of characteristics of cell pairs complements that of dynamics (Menz and Freeman 2004) by showing that coarse-to-fine connections are relatively stronger than fine-to-coarse types.

Our study shows that the presynaptic cell more frequently has a higher disparity frequency and smaller disparity range (fine-to-coarse) compared with the postsynaptic cell. However, when the presynaptic cell has a larger disparity range (coarse-to-fine), the connection strength tends to be much stronger compared with the more common situation with a presynaptic cell that has a smaller range. Thus the fine-to-coarse connection is more common, but the coarse-to-fine connection is stronger. We propose that pooling across spatial scale can explain both types of connection. The postsynaptic cell has disparity tuning that is a weighted sum of its inputs. More weight is given to the less common coarse-to-fine connection; less weight is given to the more common fine-to-coarse connection. Both coarse-to-fine and fine-to-coarse mechanisms coexist with disparity averaging. The psychophysics literature contains studies supporting coarse-to-fine (Glennerster 1996; Rohaly and Wilson 1993; Watt 1987; Wilson et al. 1991) and fine-to-coarse processing (Smallman 1995) and disparity averaging (Rohaly and Wilson 1994). Certain tasks may emphasize particular pathways, but all three mechanisms are compatible. Pooling across spatial scale is desirable to disambiguate disparity signaled by one cell (Fleet et al. 1996). If there is a temporal bias for low frequencies having shorter latencies, then pooling across scale also produces a temporal coarse-to-fine mechanism as described in the preceding paper (Menz and Freeman 2004).

ACKNOWLEDGMENTS

We thank L.E. Holm for technical support.

GRANTS

This work was supported by research and CORE grants (EY-01175 and EY-03716) from the National Eye Institute.

REFERENCES

**Adelson EH and Bergen JR.** Spatiotemporal energy models for the perception of motion. *J Opt Soc Am A* 2: 284–299, 1985.

**Aertsen AM and Gerstein GL.** Evaluation of neuronal connectivity: sensitivity of cross-correlation. *Brain Res* 340: 341–354, 1985.

**Alonso JM and Martinez LM.** Functional connectivity between simple cells and complex cells in cat striate cortex. *Nat Neurosci* 1: 395–403, 1998.

**Anzai A, Ohzawa I, and Freeman RD.** Neural mechanisms underlying binocular fusion and stereopsis: position versus phase. *Proc Natl Acad Sci USA* 94: 5438–5443, 1997.

**Anzai A, Ohzawa I, and Freeman RD.** Neural mechanisms for encoding binocular disparity: receptive field position versus phase. *J Neurophysiol* 82: 874–890, 1999a.

**Anzai A, Ohzawa I, and Freeman RD.** Neural mechanisms for processing binocular information. I. Simple cells. *J Neurophysiol* 82: 891–908, 1999b.

**Anzai A, Ohzawa I, and Freeman RD.** Neural mechanisms for processing binocular information. II. Complex cells. *J Neurophysiol* 82: 909–924, 1999c.

**Appelle S.** Perception and discrimination as a function of stimulus orientation: the "oblique effect" in man and animals. *Psychol Bull* 78: 266–278, 1972.

**Arnett D and Spraker TE.** Cross-correlation analysis of the maintained discharge of rabbit retinal ganglion cells. *J Physiol* 317: 29–47, 1981.

**Backus BT, Banks MS, van Ee R, and Crowell JA.** Horizontal and vertical disparity, eye position, and stereoscopic slant perception. *Vision Res* 39: 1143–1170, 1999.

**Barlow HB, Blakemore C, and Pettigrew JD.** The neural mechanism of binocular depth discrimination. *J Physiol* 193: 327–342, 1967.

**Berends EM and Erkelens CJ.** Strength of depth effects induced by three types of vertical disparity. *Vision Res* 41: 37–45, 2001.

**Bishop PO, Kozak W, and Vakkur GJ.** Some quantitative aspects of the cat's eye: axis and plane of references, visual field coordinates, and optics. *J Physiol* 163: 466–502, 1962.

**Brosch M and Schreiner CE.** Correlations between neural discharges are related to receptive field properties in cat primary auditory cortex. *Eur J Neurosci* 11: 3517–3530, 1999.

**Cumming BG and Parker AJ.** Binocular neurons in V1 of awake monkeys are selective for absolute, not relative, disparity. *J Neurosci* 19: 5602–5618, 1999.

**Cumming BG and Parker AJ.** Local disparity not perceived depth is signaled by binocular neurons in cortical area V1 of the macaque. *J Neurosci* 20: 4758–4767, 2000.

**Das A and Gilbert CD.** Topography of contextual modulations mediated by short-range interactions in primary visual cortex. *Nature* 399: 655–661, 1999.

**DeAngelis GC, Ghose GM, Ohzawa I, and Freeman RD.** Functional micro-organization of primary visual cortex: receptive field analysis of nearby neurons. *J Neurosci* 19: 4046–4064, 1999.

**DeAngelis GC, Ohzawa I, and Freeman RD.** Spatiotemporal organization of simple-cell receptive fields in the cat's striate cortex. I. General characteristics and postnatal development. *J Neurophysiol* 69: 1091–1117, 1993a.

**DeAngelis GC, Ohzawa I, and Freeman RD.** Spatiotemporal organization of simple-cell receptive fields in the cat's striate cortex. II. Linearity of temporal and spatial summation. *J Neurophysiol* 69: 1118–1135, 1993b.

**DeAngelis GC, Ohzawa I, and Freeman RD.** Receptive-field dynamics in the central visual pathways. *Trends Neurosci* 18: 451–458, 1995.

**DeAngelis GC, Robson JG, Ohzawa I, and Freeman RD.** Organization of suppression in receptive fields of neurons in cat visual cortex. *J Neurophysiol* 68: 144–163, 1992.

**Fleet DJ, Wagner H, and Heeger DJ.** Neural encoding of binocular disparity: energy models, position shifts, and phase shifts. *Vision Res* 36: 1839–1857, 1996.

**Freeman RD and Ohzawa I.** On the neurophysiological organization of binocular vision. *Vision Res* 30: 1661–1676, 1990.

**Freeman RD and Ohzawa I.** Development of binocular vision in the kitten's striate cortex. *J Neurosci* 12: 4721–4736, 1992.

**Ghose GM, Freeman RD, and Ohzawa I.** Local intracortical connections in the cat's visual cortex: postnatal development and plasticity. *J Neurophysiol* 72: 1290–1303, 1994a.

**Ghose GM, Ohzawa I, and Freeman RD.** Receptive-field maps of correlated discharge between pairs of neurons in the cat's visual cortex. *J Neurophysiol* 71: 330–346, 1994b.

**Glennerster A.** The time course of 2-D shape discrimination in random dot stereograms. *Vision Res* 36: 1955–1968, 1996.

**Hata Y, Tsumoto T, Sato H, and Tamura H.** Horizontal interactions between visual cortical neurones studied by cross-correlation analysis in the cat. *J Physiol* 441: 593–614, 1991.

**Hubel DH and Wiesel TN.** Receptive fields, binocular interaction and functional architecture of the cat's visual cortex. *J Physiol* 160: 106–154, 1962.

**Kruger J and Aiple F.** Multimicroelectrode investigation of monkey striate cortex: spike train correlations in the infragranular layers. *J Neurophysiol* 60: 798–828, 1988.

**Li B, Peterson MR, and Freeman RD.** Oblique effect: a neural basis in the visual cortex. *J Neurophysiol* 90: 204–217, 2003.

**Li G.** Robust regression. In: *Exploring Data Tables, Trends, and Shapes*, edited by Hoaglin DC, Mosteller F, and Tukey JW. New York: Wiley, 1985, p. 281–340.

**Liu Z, Gaska JP, Jacobson LD, and Pollen DA.** Interneuronal interaction between members of quadrature phase and anti- phase pairs in the cat's visual cortex. *Vision Res* 32: 1193–1198, 1992.

**Marr D and Poggio T.** A computational theory of human stereo vision. *Proc R Soc Lond B Biol Sci* 204: 301–328, 1979.

**Mechler F and Ringach DL.** On the classification of simple and complex cells. *Vision Res* 42: 1017–1033, 2002.

**Menz MD and Freeman RD.** Stereoscopic depth processing in the visual cortex: a coarse-to-fine mechanism. *Nat Neurosci* 6: 59–65, 2003.

**Menz MD and Freeman RD.** Temporal dynamics of binocular disparity processing in the central visual pathway. *J Neurophysiol* 91: 1782–1793, 2004.

**Moore GP, Segundo JP, Perkel DH, and Levitan H.** Statistical signs of synaptic interaction in neurons. *Biophys J* 10: 876–900, 1970.

**Nelson JI, Salin PA, Munk MH, Arzi M, and Bullier J.** Spatial and temporal coherence in cortico-cortical connections: a cross-correlation study in areas 17 and 18 in the cat. *Vis Neurosci* 9: 21–37, 1992.

**Nikara T, Bishop PO, and Pettigrew JD.** Analysis of retinal correspondence by studying receptive fields of binocular single units in cat striate cortex. *Exp Brain Res* 6: 353–372, 1968.

**Ohzawa I, DeAngelis GC, and Freeman RD.** Stereoscopic depth discrimination in the visual cortex: neurons ideally suited as disparity detectors. *Science* 249: 1037–1041, 1990.

**Ohzawa I, DeAngelis GC, and Freeman RD.** Encoding of binocular disparity by simple cells in the cat's visual cortex. *J Neurophysiol* 75: 1779–1805, 1996.

**Ohzawa I, DeAngelis GC, and Freeman RD.** Encoding of binocular disparity by complex cells in the cat's visual cortex. *J Neurophysiol* 77: 2879–2909, 1997.

**Ohzawa I and Freeman RD.** The binocular organization of complex cells in the cat's visual cortex. *J Neurophysiol* 56: 243–259, 1986.

**Perkel DH, Gerstein GL, and Moore GP.** Neuronal spike trains and stochastic point processes. I. The single spike train. *Biophys J* 7: 391–418, 1967a.

**Perkel DH, Gerstein GL, and Moore GP.** Neuronal spike trains and stochastic point processes. II. Simultaneous spike trains. *Biophys J* 7: 419–440, 1967b.

**Poggio GF.** Cortical neural mechanisms of stereopsis studied with dynamic random- dot stereograms. *Cold Spring Harb Symp Quant Biol* 55: 749–758, 1990.

**Poggio GF and Fischer B.** Binocular interaction and depth sensitivity in striate and prestriate cortex of behaving rhesus monkey. *J Neurophysiol* 40: 1392–1405, 1977.

**Poggio GF, Motter BC, Squatrito S, and Trotter Y.** Responses of neurons in visual cortex (V1 and V2) of the alert macaque to dynamic random-dot stereograms. *Vision Res* 25: 397–406, 1985.

**Pollen DA and Ronner SF.** Phase relationships between adjacent simple cells in the visual cortex. *Science* 212: 1409–1411, 1981.

**Press WH, Teukolsky SA, Vetterling WT, and Flannery BP.** *Numerical Recipes in C.* Cambridge, UK: Cambridge Univ. Press, 1992.

**Reid RC and Alonso JM.** Specificity of monosynaptic connections from thalamus to visual cortex. *Nature* 378: 281–284, 1995.

**Ringach DL.** Spatial structure and symmetry of simple-cell receptive fields in macaque primary visual cortex. *J Neurophysiol* 88: 455–463, 2002.

**Rohaly AM and Wilson HR.** Nature of coarse-to-fine constraints on binocular fusion. *J Opt Soc Am A* 10: 2433–2441, 1993.

**Rohaly AM and Wilson HR.** Disparity averaging across spatial scales. *Vision Res* 34: 1315–1325, 1994.

**Schwarz C and Bolz J.** Functional specificity of a long-range horizontal connection in cat visual cortex: a cross-correlation study. *J Neurosci* 11: 2995–3007, 1991.

**Skottun BC, De Valois RL, Grosof DH, Movshon JA, Albrecht DG, and Bonds AB.** Classifying simple and complex cells on the basis of response modulation. *Vision Res* 31: 1079–1086, 1991.

**Smallman HS.** Fine-to-coarse scale disambiguation in stereopsis. *Vision Res* 35: 1047–1060, 1995.

**Smallman HS and MacLeod DI.** Spatial scale interactions in stereo sensitivity and the neural representation of binocular disparity. *Perception* 26: 977–994, 1997.

**Sutter EE.** The fast m-transform: a fast computation of cross-correlations with binary m-sequences. *SIAM J Comput* 20: 686–694, 1991.

**Tanaka K.** Cross-correlation analysis of geniculostriate neuronal relationships in cats. *J Neurophysiol* 49: 1303–1318, 1983.

**Watson AB and Ahumada AJ Jr.** Model of human visual-motion sensing. *J Opt Soc Am A* 2: 322–341, 1985.

**Watt RJ.** Scanning from coarse to fine spatial scales in the human visual system after the onset of a stimulus. *J Opt Soc Am A* 4: 2006–2021, 1987.

**Wilson HR, Blake R, and Halpern DL.** Coarse spatial scales constrain the range of binocular fusion on fine scales. *J Opt Soc Am A* 8: 229–236, 1991.